Chemical Engineering Science 267 (2023) 118321

Contents lists available at ScienceDirect

Chemical Engineering Science

journal homepage: www.elsevier.com/locate/ces

A novel model-based estimator for real-time prediction of insulin-on-board

Eleonora M. Aiello [a,b], Kelilah L. Wolkowicz [c], Jordan E. Pinsker [b], Eyal Dassau [a,b], Francis J. Doyle III [a,b,*]

[a] Harvard John A. Paulson School of Engineering and Applied Sciences, Harvard University, 150 Western Avenue, Boston, MA 02134, USA
[b] Sansum Diabetes Research Institute, Santa Barbara, CA, USA
[c] Department of Mechanical Engineering, University of Massachusetts Lowell, 1 University Avenue, Lowell, MA 01854, USA

HIGHLIGHTS

- People with Type 1 Diabetes need insulin injections to keep glycemia in a safe range.
- A risk can occur if the estimate of active insulin and insulin action time is not accurate.
- Current active insulin estimate does not account for physiological conditions
- Real-time estimation of active insulin can be enhanced by using an insulin sensor
- Patient-tailored active insulin estimates are obtained by an extended Kalman filter.

ARTICLE INFO

Article history:
Received 31 May 2022
Received in revised form 9 November 2022
Accepted 15 November 2022
Available online 20 November 2022

Keywords:
Type 1 Diabetes
Insulin Measurement
Kalman Filter
Insulin-On-Board

ABSTRACT

The availability of insulin measurements can improve automated insulin delivery technology for people with type 1 diabetes, who require exogenous insulin delivery. To reduce the risk of hypo- or hyperglycemia, there is a strong need of calculating the amount of insulin that is yet to become active from the previous doses, known as the insulin-on-board. In this work, we propose an approach for the real-time estimation of insulin-on-board by means of an extended Kalman filter based on actual insulin levels measured using a microchip-based immunoassay. Moreover, the availability of further insulin measurements, collected with high accuracy by the laboratory-based ELISA, allows the development of a probabilistic description of the insulin measurement error, which is exploited in the tuning of the extended Kalman filter. The proposed approach for real-time quantification of the insulin-on-board will allow an informed refinement of insulin dosing, especially under varied conditions including stress and exercise.

1. Introduction

Individuals with type 1 diabetes (T1D) require lifelong replacement of insulin to maintain healthy metabolism, prevent ketoacidosis, and maintain glucose in a desired range in order to minimize long-term disease complications. Advances in technology and closed-loop control algorithms have enabled automated insulin delivery (AID) for management of T1D (Aiello et al., 2021). One of the main limitations of current AID systems is the presence of residual insulin remaining active in the plasma, known as the insulin-on-board (IOB), which must be accounted for in order to calculate a safe amount of additional insulin to deliver. The IOB represents the estimate of the amount of insulin remaining in the body from previous insulin delivery. Currently, the residual active insulin is estimated using either a curvilinear or linear decay curve, neither of which account for any dependence on physiological conditions, such as changes in insulin sensitivity due to exercise, stress, illness, or medication use. Similarly, meals high in fat or other macronutrients could alter insulin sensitivity after a meal (Dadlani et al., 2018). Many AID designs compute an approximation of the IOB to correct for any remaining insulin from the last delivery (Rodriguez-Saldana, 2019; Gondhalekar et al., 2018). In the absence of real-time insulin measurements, glucose concentration via glucose-insulin models are used to estimate the plasma insulin concentration (Hajizadeh et al., 2017; Hajizadeh et al., 2019; De Pereda et al., 2016; Haidar et al., 2013; Dalla Man et al., 2007; Hovorka et al., 2004). The ability to measure insulin in real-time provides a unique opportunity to determine available circulating insulin in individual patients and lead to more efficient glucose regulation (Wolkowicz et al., 2021). In Wolkowicz et al.

* Corresponding author at: Harvard John A. Paulson School of Engineering and Applied Sciences, Harvard University, 150 Western Avenue, Boston, MA 02134, USA.
E-mail address: frank_doyle@seas.harvard.edu (F.J. Doyle III).

https://doi.org/10.1016/j.ces.2022.118321
0009-2509/

(2020), a fully *in silico* Kalman filter was developed to enable the reconstruction of plasma insulin concentration utilizing a noisy remote compartment, while in Hajizadeh et al. (2019), De Pereda et al. (2016) an extended and an unscented Kalman filter algorithms are used to estimate the plasma insulin concentration.

For the first time, the applicability of a microneedle insulin immunosensor as a point of care (POC) device was evaluated by conducting validation tests in adults with T1D at the clinical research unit at the Sansum Diabetes Research Institute, Santa Barbara, CA (Vargas et al., 2022; Aiello et al., 2022). This proof-of-concept study showed the feasibility for near real-time evaluation of insulin levels and boosted the investigation of how to exploit the measurements of insulin levels to improve diabetes management. The novel sensor can measure insulin levels in untreated serum samples obtained from venous blood, which can be used to estimate plasma insulin concentration and, eventually, personalized IOB curves that would help avoid over-delivery of insulin, thus minimizing the risk for hypoglycemia. While free insulin represents a portion of total insulin unbound by insulin binding antibodies in circulation, and provides an important indicator of the relationship between insulin levels and blood glucose, the novel microneedle sensor uses only a very small sample of fluid and it was not yet feasible to measure free insulin with the sensor. In order to achieve the goal of residual active insulin estimation, we propose the design of an extended Kalman filter (EKF) that utilizes measurements from the insulin immunosensor to estimate plasma insulin concentration, even in the case of infrequent measurements. Addtionally, an error model for the insulin immunosensor was developed to characterize the uncertainties in the insulin measurements and, in turn, improve the tuning of the EKF. The EKF was chosen as the observer because it supports a real-time model for making estimates of the current insulin state.

Beginning with the initial pathway of subcutaneous insulin administration to plasma from Wolkowicz et al. (2020), Schiavon et al. (2017), the patient-specific insulin pharmacokinetic (PK) model is enhanced by the introduction of a capillary compartment because capillaries are the connectors between arterial and venous blood. Insulin levels were measured as the venous level, which show a difference compared with arterial levels. Levels are higher in the arterial blood because insulin diffuses from the plasma to interstitial fluid (ISF) as blood circulates through the capillary system (Cengiz and Tamborlane, 2009). Subsequently, the insulin pathway from the capillaries to the ISF insulin compartment is expanded in a barrier-limited and flow-limited condition (Sangren and Sheppard, 1953; Goresky et al., 1970; Bassingthwaighte, 1974). Additionally, the formulation of the insulin plasma clearance is replaced by a saturable nonlinear function. In Rasmussen et al. (2011), Lindauer and Becker (2019), the authors state that the elimination of insulin in plasma is not only a first-order process, but a saturable nonlinear net elimination. In Wagner (1973), the insulin degradation rate via saturable Michaelis–Menten kinetics is suggested, since the absorption rate in the plasma depends on the concentration in the subcutis, as well as on the concentration gradient over the capillary wall.

Moreover, in order to facilitate the tuning of the EKF, a model of the probabiliy density function (PDF) of the immunosensor measurement error model is derived. Specifically, immunosensor measurement error data are derived as the difference between the measurements obtained by the microneedle insulin immunosensor and the reference insulin values obtained via the centralized laboratory-based ELISA method, and a PDF estimated from such data. In the framework of self-monitoring blood glucose (SMBG) measurements, the error distribution has been described by a Gaussian distribution with constant mean and standard deviation over the entire glucose range (Boyd and Bruns, 2009; Breton and Kovatchev, 2010; Virdi and Mahoney, 2012), while a SMBG error model based on a ensemble of distributions been developed and validated in Vettoretti et al. (2015). A similar approach is adopted in this work for insulin measurements, as it well suits the requirements of the EKF.

As an overview, this paper has four main contributions:

- an extended model for the insulin PK dynamics that integrates a capillary compartment,
- a probabilistic description of the insulin immunosensor measurement error for characterizing the uncertainties in the measurements,
- the design of an EKF that utilizes measurements from the insulin immunosensor to estimate plasma insulin concentration, and,
- a novel methodology to calculate patient-tailored active insulin based on the EKF state estimates.

The parameters of the PK model are obtained from the literature (Schiavon et al., 2017; Kovatchev et al., 2010; Vicini et al., 2014), or, when not available, estimated by the EKF. The available measurement samples from the immunosensor collected during the clinical study at the Sansum Diabetes Research Institute, Santa Barbara, CA (Vargas et al., 2022; Aiello et al., 2022) are used as measurement signals in the EKF. The performance of the EKF is demonstrated on the protocols of the clinical study by assessment of the concordance with both the immunosensor and ELISA insulin levels computing root-mean-square error (RMSE).

2. Material and methods

2.1. Insulin pharmacokinetic model

Starting from the model in Schiavon et al. (2017), which models the subcutaneous (SC) absorption of fast-acting insulin, the insulin concentration in the SC compartments are defined as:

$$\begin{aligned} \dot{I}_{SC1} &= -(k_{a1} + k_d) I_{SC1} + u(t-\tau) \\ \dot{I}_{SC2} &= -k_{a2} I_{SC2} + k_d I_{SC1} \end{aligned} \tag{1}$$

where I_{SC1} [pmol/kg] is the first SC compartment representing insulin in a non-monomeric state, while I_{SC2} [pmol/kg] represents insulin in the monomeric state. The parameter k_d [min^{-1}] is the transfer rate from I_{SC1} into I_{SC2}, while the rate constants k_{a1} and k_{a2} [min^{-1}] represent the non-monomeric and monomeric insulin absorption into plasma, respectively. The model parameters are reported in Schiavon et al. (2017), Kovatchev et al. (2010). In Schiavon et al. (2017), the inflow in the plasma compartment is determined by insulin, which is finally absorbed from I_{SC1} and I_{SC2}, while the net elimination of insulin in plasma was assumed to be linear. In this work, a saturable Michaelis–Menten kinetics is assumed to describe the insulin plasma elimination given by:

$$\frac{k_1 I_P}{k_2 + I_P} \tag{2}$$

where I_P [pmol/kg] represents insulin in the plasma, k_1 [min^{-1}] is the constant representing the maximum insulin clearance rate and k_2 [pmol/kg] is the half-saturation value. The dynamics of the plasma compartement can be written as follows:

$$\dot{I}_P = k_{a1} I_{SC1} + k_{a2} I_{SC2} - \frac{k_1 I_P}{k_2 + I_P}. \tag{3}$$

In an effort to further examine insulin diffusion, the insulin PK model is extended to integrate the capillary exchange model between plasma and ISF insulin compartments. A two-region capillary-ISF model is applied (Vicini et al., 2014). The transport along capillaries is modelled as the flow carrying a concentration

of a substance across a surface within two regions, which are capillary plasma (I_{CAP}) and ISF (I_{ISF}), respectively (Sangren and Sheppard, 1953; Goresky et al., 1970; Bassingthwaighte, 1974). The diffusion from I_{CAP} and I_{ISF} is defined by the following partial differential equations (PDEs) as a function of time and one spatial dimension:

$$\begin{aligned} \frac{\partial I_{CAP}}{\partial t} &= D_{CAP}\frac{\partial^2 I_{CAP}}{\partial x} - \frac{FL}{V_i}\frac{\partial I_{CAP}}{\partial x} - \frac{P_s+G_{CAP}}{V_i}I_{CAP} \\ \frac{\partial I_{ISF}}{\partial t} &= D_{ISF}\frac{\partial^2 I_{ISF}}{\partial x} - \frac{P_s+G_{ISF}}{V_i}I_{ISF} + \frac{P_s}{V_i}I_{CAP} \end{aligned} \tag{4}$$

where the terms $\frac{\partial^2 I_{CAP}}{\partial x}$ and $\frac{\partial^2 I_{ISF}}{\partial x}$ model the diffusion processes in the two regions with corresponding diffusion rates D_{CAP} [$cm^2 s^{-1}$] and D_{ISF} [$cm^2 s^{-1}$]. The term FL/V_i represents the convective velocity, which can be expressed as a function of the flow in the capillary channel F [$cm^3\ s^{-1}$], the length L [cm] and the volume of distribution V_i [mL] of the capillary region. P_s [$cm^3\ g^{-1}\ s^{-1}$] is the permeability-surface area product of the capillary membrane representing the exchange rate between the regions, and G_{CAP} [$cm^3\ g^{-1}\ s^{-1}$] and G_{ISF} [$cm^3\ g^{-1}\ s^{-1}$] are the clearance rates within a region (Bassingthwaighte et al., 1986). A detailed description of the two-region capillary-ISF model can be found in Vicini et al. (2014).

The two-region capillary-ISF model is included in the EKF. It is worthy to highlight that PDEs cannot be used in the formulation of the EKF. A preliminary step is required to convert the PDEs into a set of ordinary differential equations (ODEs). Using Euler's method (Brasseur and Jacob, 2017), the PDEs can be recast as follows (Poulain et al., 1997):

$$\dot{I}_{CAP} = D_{CAP}\frac{I_{CAP} - 2I_P/V_P}{L^2} - \frac{FL}{V_i}\frac{I_{CAP} - I_P/V_P}{L} - \frac{P_s + G_{CAP}}{V_i}I_{CAP} \tag{5}$$

$$\dot{I}_{ISF} = D_{ISF}\frac{I_{ISF} - 2I_{CAP}}{L^2} - \frac{P_s + G_{ISF}}{V_i}I_{ISF} + \frac{P_s}{V_i}I_{CAP}. \tag{6}$$

where V_P is the plasma distribution volume. Additionally, insulin clearance in I_{ISF} due to the insulin action on the peripheral glucose utilization is added in Eq. 6 as follows:

$$\dot{I}_{ISF} = D_{ISF}\frac{I_{ISF} - 2I_{CAP}}{L^2} - \frac{P_s + G_{ISF}}{V_i}I_{ISF} + \frac{P_s}{V_i}I_{CAP} - p_{2U}I_B. \tag{7}$$

where p_{2U} is the rate constant of insulin action on the peripheral glucose utilization and I_B is basal insulin.

2.2. Immunosensor measurement error model

The novel disposable insulin electrochemical sensor was developed in controlled lab settings at the University of California San Diego. It can provide near real-time insulin detection in a microliter sample of undiluted serum using a microchip-based immunoassay (Vargas et al., 2022). The immunostrips were applied for on-the-spot insulin determination in untreated serum samples from venous blood collected from nine individuals with T1D. For validation purposes, the insulin concentrations were also quantified by a laboratory-based ELISA assay. To identify the model of the PDF of the immunosensor measurement error, errors are computed for the sample dataset as follows:

$$E = Y - X \tag{8}$$

where E is the error between Y and X representing the insulin immunosensor concentrations and the measurements obtained by the ELISA method, respectively.

Since the PDF of immunosensor measurement error is formulated to characterize the error noise covariance in the EKF, we are interested in testing the normality of E to check whether the EKF assumption on having the measurement noise normally distributed is satisfied (Rawlings et al., 2017). To this end, the Kolmogorov–Smirnov (KS) and Shapiro–Wilk (SW) test of normality with significance level 0.05 is applied to E. If the null hypothesis of normality fails to be rejected, a Normal PDF is fitted by maximum likelihood estimation (MLE).

2.3. Extended Kalman Filter

An EKF insulin observer was developed by combining Eq. 1 with Eqs. 3, 5, and 7. The nonlinear term in Eq. 3 has two unknown parameters k_1 and k_2. To jointly estimate the system states and the unknown parameters, fictitious parameter dynamics are introduced with the assumption that k_1 and k_2 are constant values. To maintain consistent with (Wolkowicz et al., 2020), I_B is added as a state for parameter estimation in the following continuous-time model:

$$\begin{bmatrix} \dot{I}_{SC1} \\ \dot{I}_{SC2} \\ \dot{I}_P \\ \dot{I}_{CAP} \\ \dot{I}_{ISF} \\ \dot{I}_B \\ \dot{k}_1 \\ \dot{k}_2 \end{bmatrix} = \begin{bmatrix} -(k_{a1}+k_d)I_{SC1} + u(t-\tau) \\ -k_{a2}I_{SC2} + k_d I_{SC1} \\ k_{a1}I_{SC1} + k_{a2}I_{SC2} - \frac{k_1 I_P}{k_2 + I_P} \\ D_{CAP}\frac{I_{CAP}-2I_P}{L^2} - \frac{FL}{V_i}\frac{I_{CAP}-I_P}{L} - \frac{P_s+G_{CAP}}{V_i}I_{CAP} \\ D_{ISF}\frac{I_{ISF}-2I_{CAP}}{L^2} - \frac{P_s+G_{ISF}}{V_i}I_{ISF} + \frac{P_s}{V_i}I_{CAP} - p_{2U}I_B \\ 0 \\ 0 \\ 0 \end{bmatrix} \tag{9}$$

The continuous-time model was discretized via forward Euler integration, obtaining the following discrete-time state-space equations (Rawlings et al., 2017):

$$\begin{aligned} x_{k+1} &= f(x_k, u_{k-\Delta t\tau}) + w_k^{EKF} \\ y_k &= g(x_k, u_{k-\Delta t\tau}) + v_k^{EKF} \end{aligned} \tag{10}$$

where x is the state vector of the insulin concentration in each compartment, u is the insulin dose, y is the measured state (i.e., the ISF concentration), $f(\cdot)$ is the model dynamic equation, and $g(\cdot)$ is the model output transformation equation. The model sampling time Δt corresponds to five minutes. Note that Δt should not be confused with the measurement sampling time, which represents the time points when insulin measurements were available, i.e., at mealtime and at 1, 2, and 4 h after the mealtime. Process and measurement noises, w_k^{EKF} and v_k^{EKF}, are defined as follows:

$$\begin{aligned} w_k^{EKF} &\sim N\left(0, Q^{EKF}\right) \\ v_k^{EKF} &\sim N\left(0, R^{EKF}\right) \end{aligned} \tag{11}$$

where Q^{EKF} is the process noise covariance and R^{EKF} is the measurement noise covariance. Note that the latter was determined from the immunosensor error model described in Section 2.2 to accurately represent the specific sensor noise levels.

Once the discretized model has been defined, the state and measurement Jacobian matrices, $\widehat{A}_k$ and $\widehat{C}_k$, respectively, are obtained by linearizing the system dynamics and output transformation models about the point $(\hat{x}_{k|k}, u_k)$, as follows:

$$\widehat{A}_k = \frac{df(x,u)}{dx}\Big|_{\hat{x}_{k|k},u_k} \text{ and } \widehat{C}_k = \frac{dg(x,u)}{dx}\Big|_{\hat{x}_{k|k},u_k} \tag{12}$$

where $\hat{x}_{k|k}$ is the propagated and updated state from the previous time step and u_k is the most recent insulin delivery. The EKF prediction step can be carried out as follows:

$$\begin{aligned} \hat{x}_{k+1|k} &= f\left(x_{k|k}, u_{k-\Delta t\tau}\right) + 0 \\ P_{k+1|k} &= \widehat{A}_k P_{k|k} \widehat{A}_k^T + Q^{EKF} \end{aligned} \tag{13}$$

where $\hat{x}_{k+1|k}$ represents the propagated state at the current time step and $P_{k+1|k}$ is the state covariance matrix. The measurement,

or correction, step for the state estimate and covariance is then performed using the following equations:

$$\begin{aligned} K_{k+1} &= \widehat{A}_k P_{k+1|k} \widehat{C}_k^T \left[\widehat{C}_k P_{k+1|k} \widehat{C}_k^T + R^{EKF} \right]^{-1} \\ \hat{x}_{k+1|k+1} &= \hat{x}_{k+1|k} + K_{k+1}[y_k - g(\hat{x}_{k+1|k}k, u_{k-\Delta t\tau})] \\ P_{k+1|k+1} &= [I - K_{k+1} \widehat{C}_k P_{k+1|k}] \end{aligned} \tag{14}$$

where K is the optimal EKF gain, which minimizes the residual error and is dependent upon the current estimation through $\widehat{A}_k$ and $\widehat{C}_k$.

2.4. Real-time prediction of the active insulin in the plasma

To compute the real-time prediction of the percent insulin remaining active in the plasma, the Wagner–Nelson method is considered in combination with the EKF estimates. This approach allows the accurate estimation of the rate of a generic drug absorption in the plasma from its elimination rate (Wagner, 1974). In case of a single dose case, the mass balance in the plasma compartment yields:

$$X_A = X_P + X_E \tag{15}$$

where $X_A$is the cumulative mass of the absorbed dose, X_P is the mass of present in the plasma, and X_E is the cumulative mass of the drug eliminated. In insulin treatment, a single-dose framework can be applied to the insulin bolus administered to compensate for the carbohydrate content of a meal. However, the insulin pump continuously delivers the basal rate, which corresponds to a constant insulin infusion. For the hypothesis of the single dose to be valid, the estimated I_B is subtracted from I_P as follows:

$$I_P^B = I_P/V_P - I_B \tag{16}$$

where V_P is the plasma distribution volume. Differentiating Eq. 15 and substituting with $X_P = V_P I_P^B$:

$$\dot{X}_A = V_P \dot{I}_P^B + \dot{X}_E. \tag{17}$$

The rate of insulin elimination in the plasma $\dot{X}_E$ corresponds to $V_P \frac{k_1 I_P^B}{k_2 + I_P^B}$ in the PK model. To compute the cumulative mass of the absorbed insulin dose from the time the dose was administered, T_0, until a generic time instant T, Eq. 17 is integrated from $t = T_0$ to T:

$$\int_{T_0}^{T} \dot{X}_A(\tau) d\tau = \int_{T_0}^{T} V_P \dot{I}_P^B(\tau) d\tau + \int_{T_0}^{T} V_P \frac{k_1 I_P^B(\tau)}{k_2 + I_P^B(\tau)} d\tau. \tag{18}$$

Assuming that $X_A(T_0) = 0$:

$$X_A(T) = V_P I_P^B(T) - V_P I_P^B(T_0) + AUC_{T_0}^{T} \left(V_P \frac{k_1 I_P^B}{k_2 + I_P^B} \right) \tag{19}$$

since the integral corresponds to the area under the plasma insulin level versus time curve. If $T = \infty$, the total amount of insulin ultimately absorbed is:

$$X_A(\infty) = AUC_{T_0}^{\infty} \left(V_P \frac{k_1 I_P^B}{k_2 + I_P^B} \right) \tag{20}$$

where it can be assumed that the plasma insulin concentration returns to initial level when the dose is ultimately absorbed, i.e. $I_P^B(T_0)$ and $I_P^B(\infty)$ are equal. The percent insulin remaining to be absorbed $I\hat{O}B(T)$ can be computed at each time instant T as:

$$I\hat{O}B(T) = 1 - \frac{X_A(T)}{X_A(\infty)} 100. \tag{21}$$

The Wagner-Nelson calculation can be extend in cases of multiple doses by subtracting the initial plasma concentration when a dose is administered. In this work, the main focus is on the single-dose case to remain consistent with the study protocol applied to evaluate the insulin immunosensor. During the study, participants were given an injection of their usual mealtime insulin before eating breakfast and no bolus insulin was given within 6 h of the breakfast dose (Aiello et al., 2022).

3. Results and discussion

3.1. Insulin error model identification and validation

Fig. 1(a) shows the original 34 paired samples, where it appears that an outlier sample of X of 374 $\mu iU/mL$ was recorded by ELISA method due to the presence of high anti-insulin antibodies, which can impact accurate measurement of insulin levels. The impact of autoantibody titers on the accuracy of the sensor insulin measurement still needs to be determined. For this reason, this sample was not used for modeling. The null hypothesis of E being normally distributed for KS and SW tests failed to be rejected with p-values of 0.44 and 0.10, respectively, thus a normality assumption for the immunosensor error model was assumed to be fulfilled. The estimated PDF, which was fitted by MLE to the error data is reported in Fig. 1(b) on top of the data histogram. The estimated PDF shows a near-zero mean and a standard deviation of 49 $\mu iU/dL$. The identified distribution well approximates the zero mean and a non-null standard deviation assumptions on v_k^{EKF}. Hence, the identified error model can be applied to characterize the measurement noise covariance R^{EKF} in the EKF.

3.2. Evaluation of the insulin observer

The EKF was evaluated on each participant's protocol where infrequent sensor measurements were recorded. As mentioned in Section 3.1, the EKF measurement noise standard deviation R^{EKF} was defined as 335 pmol/L, which corresponds to 49 μiU/dL. The covariance matrix Q^{EKF} has been set as follows:

$$Q^{EKF} = diag(200000, 200000, 0, 0, 0, 1000, 1000, 100)$$

The uncertainties affecting the dynamics of I_{SC1} and I_{SC2} mean to increase the reactivity to any minimal input variation. The uncertainties in the dynamics of I_P are indirectly characterized by adding uncertainties on the states k_1 and k_2, which are the unknown parameters characterizing the insulin plasma elimination and are the last two values of Q^{EKF}. While the description of the dynamic behavior of I_{CAP} and I_{ISF} is assumed to be correct, the uncertainties in the dynamics of I_B represent the mismatch with the basal insulin of the real patient.

The performance of the EKF was evaluated using the clinical study protocols adopted at the Sansum Diabetes Research Institute, Santa Barbara, CA (Aiello et al., 2022), listed in Table 1. We aim for a one-to-one comparison with the individual participant data, but the PK model parameters are unknown for specific subjects in the clinical study, nor can they be estimated from the available data. The unknown parameters are obtained from the *in silico* adult population of the United States Food and Drug Administration-accepted University of Virginia (UVA)/Padova T1D Metabolic Simulator (Visentin et al., 2018). Two *in silico* population options are available within the Simulator: 1) utilize the average parameters of the *in silico* population or 2) utilize the ten *in silico* patient-specific sets of parameters and average the EKF estimates. We opted for the latter choice because it allows an uncertainty characterization of the estimates. A EKF estimate for each *in silico* patient is computed and the median and interquartile (IQR) ranges of the state estimates are taken as final results. The EKF was initialized

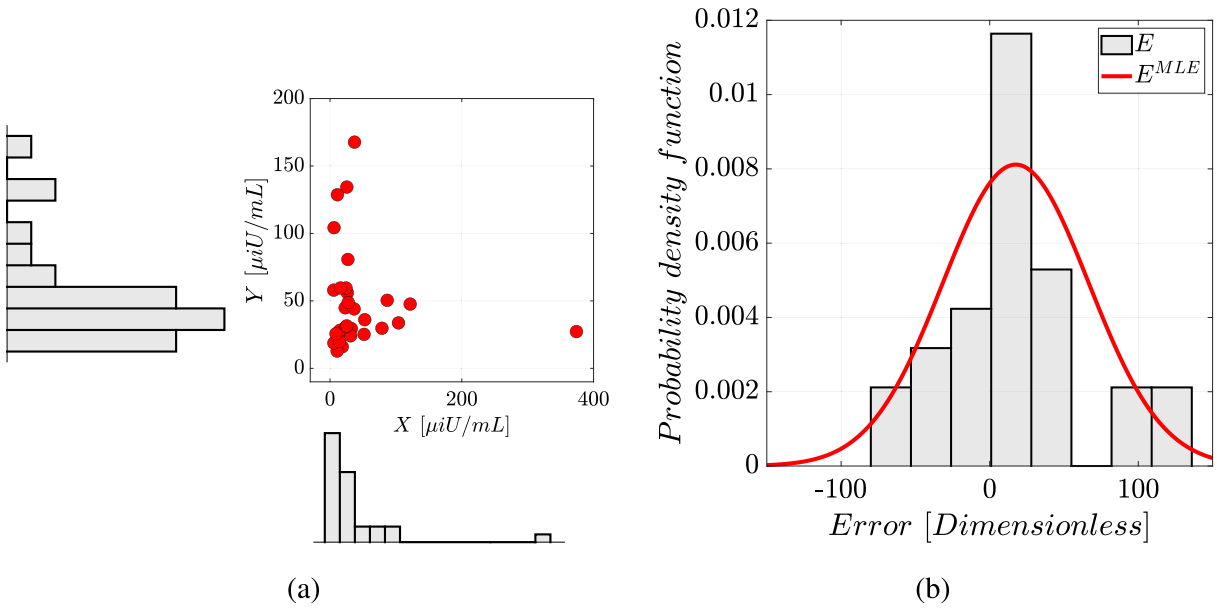

Fig. 1. a: Scatterplot for the insulin concentrations obtained by decentralized immunosensor (Y) and a centralized ELISA method (X), with its marginal distributions as univariate histograms. **b**: Histogram reporting on the x-axis of the measurement error data, while the probability density function of the samples is reported on the y-axis. The estimated Normal distribution in represented by the red line.

Table 1
The protocols adopted during the clinical study reported in Aiello et al. (2022).

Participant	Scenario
HS1-02	27 grams carbohydrates at 08:22
HS1-03	60 grams carbohydrates at 08:13
HS1-04	45 grams carbohydrates at 08:23
HS1-05	20 grams carbohydrates at 07:20
HS1-06	20 grams carbohydrates at 07:32
HS1-07	20 grams carbohydrates at 07:32
HS1-08	60 grams carbohydrates at 08:03
HS1-09	70 grams carbohydrates at 07:58

with known individualized values of the *in silico* adult population from the UVA/Padova T1DM Metabolic Simulator (Visentin et al., 2018), with the exception of k_1 and k_2. The initialization of the unknown parameters k_1 and k_2 plays a key role in the convergence of the EKF. Specifically, the ratio k_1/k_2 is responsible for the net insulin elimination dynamics. Greater values for k_2 compared to k_1 correspond to a faster net elimination, while smaller values for both k_1 and k_2 affect the excursion of the plasma insulin concentration, which increases abnormally. Based on this consideration, the two parameters were initialized as 50 $\left[min^{-1}\right]$ and 150 $\left[min^{-1}\right]$, respectively.

The participants' measurement samples from the immunosensor are used as measurements in the state estimation when available, i.e., at baseline before breakfast, then at 60, 120, and 240 min after mealtime. The EKF estimates are compared with the insulin measurements collected by the insulin immunosensor, as well as the laboratory-based ELISA insulin measurements. Given the presence of insulin antibodies in some participants and differences in baseline insulin levels across the nine participants (Aiello et al., 2022), concordance of the EKF with both the immunosensor and ELISA insulin levels was assessed in the evaluation of changes from baseline by computing RMSE to determine the prediction errors from the actual insulin measurements.

Please note that participant HS1-01 was not included because the baseline measurement was not obtained via the immunosensor. Additionally, the four-hour insulin measurement for HS1-02 is missing due to issues related to immunostrip transportation conditions.

For each participant, Fig. 2 presents the median and IQR ranges of the estimated I_{ISF}, with the available measurement samples from the immunosensor and serum samples extracted from venous blood via ELISA method, as well as the corresponding delta changes from baseline. In Fig. 2, it is observed that the estimates of the I_{ISF} show similar temporal trends to those of ELISA insulin levels for all the participants, characterized by a rise in insulin levels after insulin injection, a peak within the first hour and then a decrease over the next three to four hours. Participants HS1-08 and HS1-09 had much higher insulin concentrations estimated by the immunosensor relative to ELISA. It is important to note that the EKF state estimates are consistent with the insulin levels obtained by the ELISA method, due to the underlying detailed PK model and the tuning of both the Q^{EKF} and R^{EKF} matrices. The updated EKF model yielded accurate insulin concentration estimates, as well as filtered measurement values that were outside the expected insulin concentration range. This result stresses the role of a precise sensor noise approximation in the EKF tuning process.

For each participant, the median RMSE values between the reference delta and the estimated delta changes are reported in Table 2 across three different time intervals. The median (IQR) RMSE across the participants are of 14.78 (16.34) μiU/mL, 10.88 (14.40) μiU/mL, and 6.20 (4.41) μiU/mL is observed for increasing measurement sampling intervals from 1 h to 4 h, respectively when comparing with the venous blood samples from the ELISA method, while the median and (IQR) RMSE values are 10.96 (22.66) μiU/mL, 4.87 (12.17) μiU/mL, and 5.12 (6.08) μiU/mL when comparing the immunosensor measurements. The RMSE between the estimated ISF insulin concentration from EKF and the venous insulin levels for Participant HS1-05 is affected by substantially greater levels assessed by the ELISA method at the baseline.

3.3. Verification and Use of the real-time IOB Estimate

Fig. 3 presents the median and IQR ranges of the estimated percentage of active insulin from the mealtime bolus for each partic-

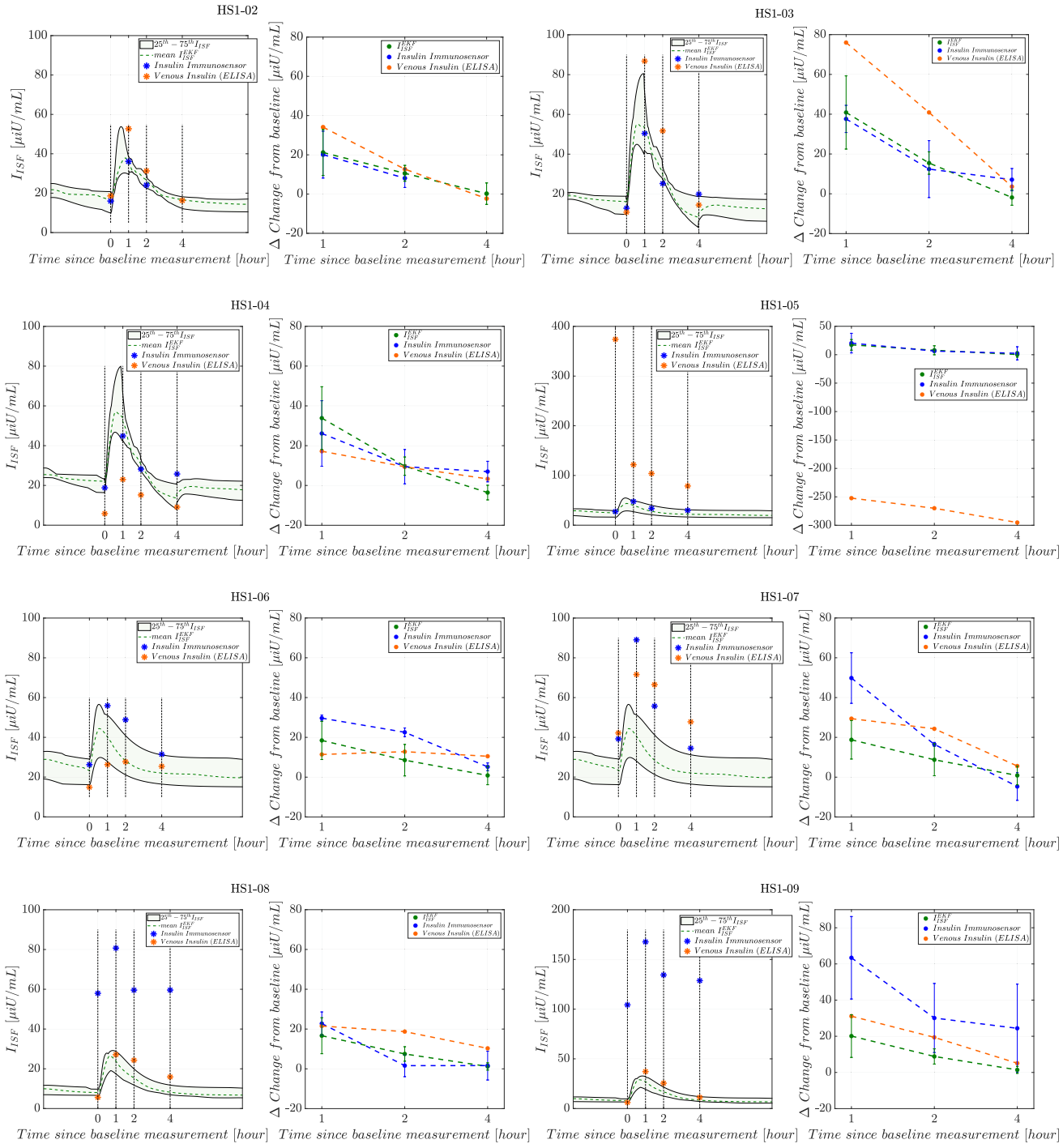

Fig. 2. On the left of each two-plot pair, median and interquartile ranges of estimated ISF insulin concentration (green line) with insulin concentrations obtained by the decentralized immunosensor (blue star) and a centralized ELISA method (orange circle) at time samples of 1-, 2-, and 4-h intervals at a noise standard deviation of 49 $\mu iU/mL$. On the right, median delta change from baseline of insulin concentrations estimated by the insulin observer (green star) with the measurements obtained by the decentralized immunosensor (blue cirle) and a centralized ELISA method (orange circle). Error bars of insulin observer and immunosensor measurements are also included at each delta.

ipant. Thus, zero percentage in Fig. 3 conveys that the mealtime insulin bolus has been completely utilized by the body. Because the subject-specific reference IOB curves do not exist, we propose to validate the obtained curves indirectly, by using the blood glucose (BG) levels, since a decrease in the BG levels is expected to be seen due to the insulin utilization when the IOB curve reaches zero percentage. It is important to highlight that the BG measurements, which are reported in Fig. 4, were not used in any step of the model development and are suitable for validation purposes. Moreover, the information of the current BG level combined with the real-time IOB estimate can help for a more informed decision-making strategy to adjust the insulin therapy. If the BG levels remain elevated after an insulin bolus, the IOB estimate may suggest either increasing the insulin dose, or keeping

Table 2
EKF median RMSE [μiU/mL] at each time point when insulin measurements were available, i.e., at 1, 2, and 4 h after the mealtime measurement.

Participant	Insulin immunosensor [μiU/mL]			Venous insulin (ELISA) [μiU/mL]		
	1 h	2 h	4 h	1 h	2 h	4 h
HS1-02	1.086	2.474	-	12.914	2.126	2.504
HS1-03	3.253	3.049	8.943	35.127	25.441	5.463
HS1-04	7.727	0.275	10.548	16.657	0.315	6.868
HS1-05	14.205	3.857	2.587	258.485	272.683	295.063
HS1-06	23.043	19.686	5.126	4.783	9.936	10.436
HS1-07	43.079	13.547	4.745	22.669	21.367	5.545
HS1-08	6.096	5.883	0.424	4.856	11.217	9.094
HS1-09	43.280	21.252	22.977	10.980	10.552	3.667
Median (IQR)	10.966 (22.667)	4.870 (12.176)	5.126 (6.080)	14.785 (16.334)	10.884 (14.402)	6.207 (4.415)

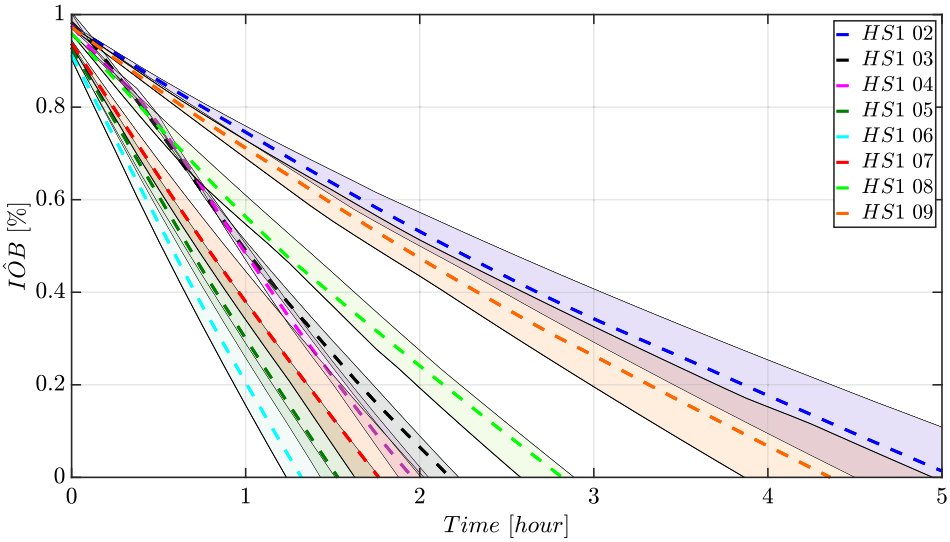

Fig. 3. Median (dashed line) and interquartile ranges of the estimated percentage of active insulin from the mealtime bolus versus time for each participant.

unchanged insulin dosing. Conversely, if an hypoglycemic state (BG $\leqslant$70 mg/dL) occurs, the IOB estimate may suggest from a slight reduction up to suspension of insulin delivery.

By looking at the IOB curve for Participant HS1-02, the insulin activity decreases at a slow rate and there is 20% of active insulin after 4 h, which clues to see the BG levels that hardly go down. In fact, the BG levels for Participant HS1-02 have a clear increasing trend for the next 5 h after mealtime, as shown in Fig. 4, though the mealtime bolus was administered and the insulin pump continued to deliver the normal basal rate. The information on the IOB estimate suggests the insulin has been almost absorbed after 4 h, although slowly, and a correction insulin bolus could be administered safely without any risk of hypoglycemia.

Similar IOB behaviors were obtained for Participants HS1-03 and HS1-04 because the insulin levels recorded by the immunosensor have similar values, although the insulin levels measured via ELISA method for Participant HS1-04 remain almost flat, while a larger excursion was recorded for Participant HS1-03, as shown in Fig. 2. However, the BG profiles of both Participants HS1-03 and HS1-04 do not present a peak due to a meal consumption and show decreasing BG levels within two hours that can be consistent with the IOB estimate, which suggests a fast utilization of the insulin bolus.

The active insulin from the mealtime bolus for Participants HS1-05 and HS1-07 is consumed quickly, consistently with the several hypoglycemic events recorded. In early morning hours, people with T1D experience the "dawn phenomenon" that refers to episodes of hyperglycemia due to an increase in insulin sensitivity. To counteract this known effect, a basal increase is recommended. Despite of being in early morning, the information on the IOB estimate could suggest a condition of insulin sensitivity, which is confirmed by the persistent low glucose levels. In this case, the estimated IOB could suggest adjusting the clinical parameters for the insulin dose to prevent a hypoglycemic state.

Although the same insulin dose was administered at mealtime, a different rate of change in the IOB is estimated for Participant HS1-06 when comparing with Participant HS1-07, suggesting a different insulin utilization rate, which can be confirmed by looking at the corresponding BG levels in Fig. 4.

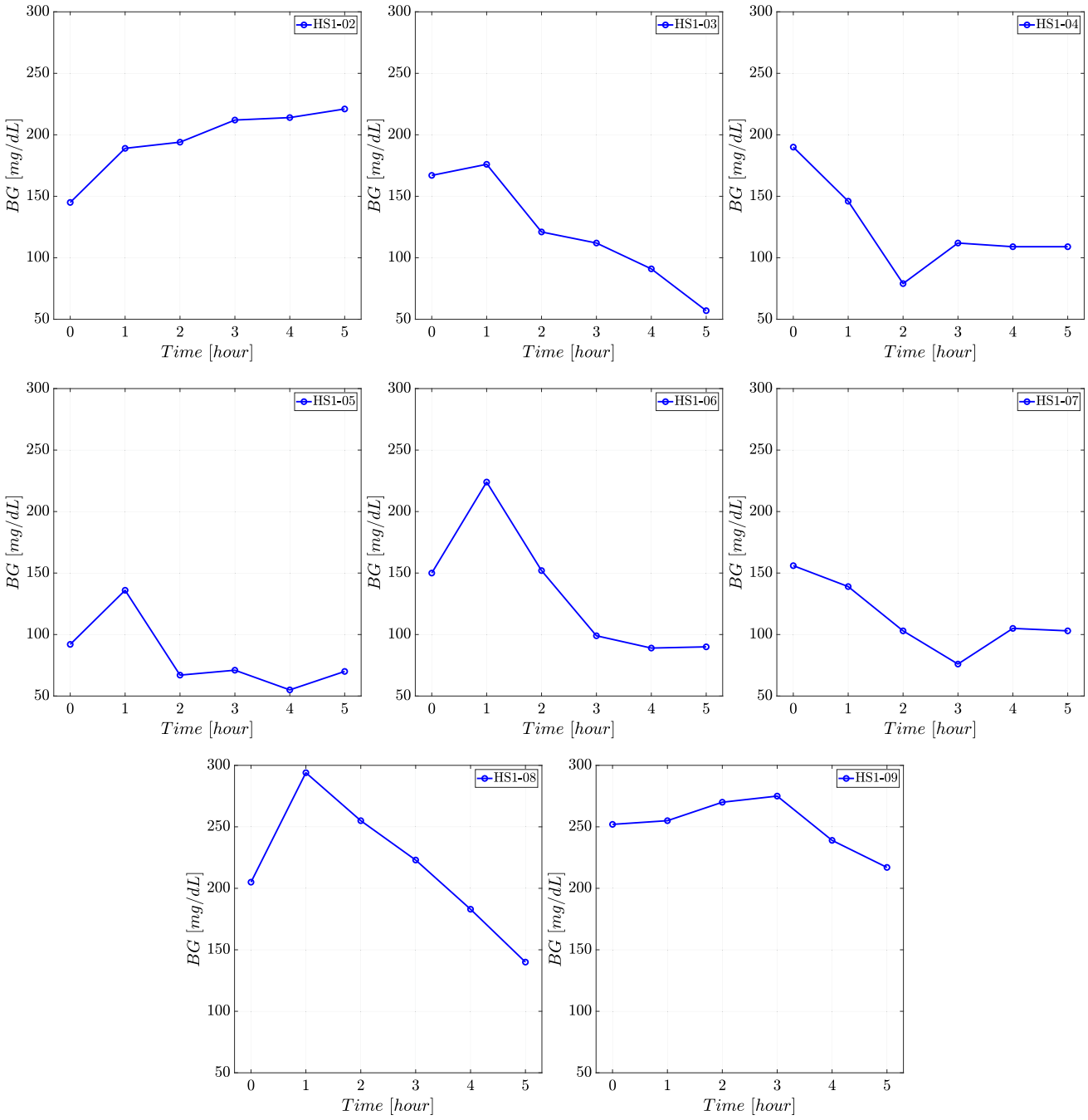

Fig. 4. Self-monitorign blood glucose (SMBG) values collected from nine subjects with T1D (Aiello et al., 2022). The SMBG values were recorded at baseline before breakfast, then every hour after the breakfast measurement within the next five hours.

Participant HS1-09 has 20% of active insulin after 3 h when glucose levels start decreasing after reaching 270 mg/dL. It may be possible to detect a change in insulin sensitivity, which in turn can be taken into account in the case of an insulin correction dose.

4. Conclusion

In this work, we propose an approach for calculating the IOB based on actual measurements of serum insulin obtained by a microneedle insulin immunoassay. Real-time measurements of ISF insulin are applied to characterize the subject-specific pharmacokinetic insulin dynamics that can be used to derive the individualized fraction of active insulin in the plasma. A model of the insulin error PDF was first derived from available measurements from the immunosensor, as well as from a laboratory-based ELISA assay. The model was then used to characterize the uncertainties in the EKF formulation leading to more accurate models for the plasma insulin concentration, which provide more precise IOB estimates. The proposed approach aims to reduce the uncertainty around IOB when dosing the insulin bolus and future work will focus on using this method to enhance the design of an augmented closed-loop automated insulin delivery system. Future research that also includes estimates of free insulin could further help to improve the utility of using IOB.

Conflict of Interest

This is the declaration of the conflict of interest.

Credit author statement

E.M.A. and K.L.W. contributed to the design and implementation of the research, to the analysis of the results, and to the writing of the manuscript. J.E.P., E.D., and F.J.D. supervised the research, contributed to the funding acquisition, and to the writing and reviewing of the manuscript. All authors approved the submitted version.

Declaration of Competing Interest

E.D. reports receiving grants from JDRF, NIH, and Helmsley Charitable Trust, personal fees from Roche and Eli Lilly, patents on artificial pancreas technology, and product support from Dexcom, Insulet, Tandem, and Roche. E.D. is currently an employee and shareholder of Eli Lilly and Company. The work presented in this manuscript was performed as part of his academic appointment and is independent of his employment with Eli Lilly and Company. F.J.D. reports equity, licensed IP and is a member of the Scientific Advisory Board of Mode AGC.The authors declare that they have no known competing financial interests or personal relationships that could have appeared to influence the work reported in this paper.

Acknowledgment

This study was funded by a grant from the Leona M. and Harry B. Helmsley Charitable Trust (2018PG-TID06). Access to the academic version of the UVA/Padova Metabolic Simulator was provided by an agreement with Prof. C. Cobelli (University of Padova) and Prof. B. P. Kovatchev (University of Virginia) for research purposes.

Nomenclature and abbreviations

Tables A.1 and A.2 list the nomenclature and the abbreviations used in this article.

Table A.1
Notation and nomenclature organized by type.

Model	Variable	Description	Units
Pharmacokinetic model	I_{SC1}	insulin in a non-monomeric state	[pmol/kg]
	I_{SC2}	insulin in the monomeric state	[pmol/kg]
	I_P	insulin in the plasma	[pmol/kg]
	I_{CAP}	insulin in capillary plasma	[pmol/L]
	I_{ISF}	insulin in interstitial fluid	[pmol/L]
	I_B	basal plasma insulin	[pmol/L]
	I_P^B	single-dose plasma insuln concentration	[pmol/L]
	k_{a1}	non-monomeric insulin absorption rate	[min^{-1}]
	k_{a2}	monomeric insulin absorption rate	[min^{-1}]
	k_d	transfer rate from I_{SC1} into I_{SC2}	[min^{-1}]
	k_1	maximum plasma insulin clearance rate	[min^{-1}]
	k_2	half-saturation plasma insulin value	[pmol/kg]
	V_P	plasma distribution volume	[L/kg]
	D_{CAP}	diffusion rate in capillary plasma	[$cm^2 s^{-1}$]
	D_{ISF}	diffusion rate in interstitial fluid	[$cm^2 s^{-1}$]
	F	flow in the capillary channel	[$cm^3\ s^{-1}$]
	L	length of the capillary region	[cm]
	V_i	volume of distribution of the capillary region	[mL]
	P_s	exchange rate between the I_{CAP} and I_{ISF}	[$cm^3\ g^{-1}\ s^{-1}$]
	G_{CAP}	clearance rate in the capillary plasma	[$cm^3\ g^{-1}\ s^{-1}$]
	G_{ISF}	clearance rate in the interstitial fluid	[$cm^3\ g^{-1}\ s^{-1}$]
	p_{2U}	insulin action rate on glucose utilization	[min^{-1}]
	X_A	cumulative mass of the absorbed insulin dose	[pmol/kg]
	X_P	mass of insulin present in the plasma	[pmol/kg]
	X_E	cumulative mass of the eliminated insulin	[pmol/kg]
Error model	X	measurements obtained by the ELISA method	[μiU/mL]
	Y	insulin immunosensor concentrations	[μiU/mL]
	E	error between Y and X	[μiU/mL]
Kalman filter	Q^{EKF}	EKF process noise covariance	[pmol/kg]
	R^{EKF}	EKF measurement noise covariance	[pmol/L]

Table A.2
Abbreviations in alphabetical order.

Abbreviation	Description
AID	automated insulin delivery
BG	blood glucose
EKF	extended Kalman filter
IOB	insulin-on-board
ISF	interstitial fluid
KS	Kolmogorov–Smirnov
MLE	maximum likelihood estimation
ODE	ordinary differential equation
PDE	partial differential equation
PDF	probability density function
PK	pharmacokinetic
POC	point of care
RMSE	root-mean-square error
SC	subcutaneous
SMBG	self-monitoring blood glucose
SW	Shapiro–Wilk
T1D	type 1 diabetes

References

Aiello, E.M., Deshpande, S., Özaslan, B., Wolkowicz, K.L., Dassau, E., Pinsker, J.E., Doyle, F.J., 2021. Review of automated insulin delivery systems for individuals with type 1 diabetes: tailored solutions for subpopulations. Curr. Opin. Biomed. Eng. 19, 100312.

Aiello, E.M., Pinsker, J.E., Vargas, E., Teymourian, H., Tehrani, F., Church, M.M., Laffel, L.M., Doyle III, F.J., Patti, M.-E., Wang, J., et al., 2022. Clinical evaluation of a novel insulin immunosensor. J. Diab. Sci. Technol. 19322968221074406.

Bassingthwaighte, J.B., 1974. A concurrent flow model for extraction during transcapillary passage. Circ. Res. 35 (3), 483–503.

Bassingthwaighte, J., Chinard, F., Crone, C., Goresky, C., Lassen, N., Reneman, R., Zierler, K., 1986. Terminology for mass transport and exchange. Am. J. Physiol.-Heart Circulat. Physiol. 250 (4), H539–H545.

Boyd, J.C., Bruns, D.E., 2009. Monte Carlo simulation in establishing analytical quality requirements for clinical laboratory tests: meeting clinical needs. Methods Enzymol. 467, 411–433.

Brasseur, G.P., Jacob, D.J., 2017. Modeling of atmospheric chemistry. Cambridge University Press.

Breton, M.D., Kovatchev, B.P., 2010. Impact of blood glucose self-monitoring errors on glucose variability, risk for hypoglycemia, and average glucose control in type 1 diabetes: an in silico study. J. Diab. Sci. Technol. 4 (3), 562–570.

Cengiz, E., Tamborlane, W.V., 2009. A tale of two compartments: interstitial versus blood glucose monitoring. Diab. Technol. Therapeut. 11 (S1), S-11.

Dadlani, V., Pinsker, J.E., Dassau, E., Kudva, Y.C., 2018. Advances in closed-loop insulin delivery systems in patients with type 1 diabetes. Curr. Diab.Rep. 18 (10), 1–10.

Dalla Man, C., Rizza, R.A., Cobelli, C., 2007. Meal simulation model of the glucose-insulin system. IEEE Trans. Biomed. Eng. 54 (10), 1740–1749.

De Pereda, D., Romero-Vivo, S., Ricarte, B., Rossetti, P., Ampudia-Blasco, F.J., Bondia, J., 2016. Real-time estimation of plasma insulin concentration from continuous glucose monitor measurements. Comput. Methods Biomech. Biomed. Eng. 19 (9), 934–942.

Gondhalekar, R., Dassau, E., Doyle III, F.J., 2018. Velocity-weighting & velocity-penalty mpc of an artificial pancreas: Improved safety & performance. Automatica 91, 105–117.

Goresky, C.A., Ziegler, W.H., Bach, G.G., Wangel, B., 1970. Capillary exchange modeling: Barrier-limited and flow-limited distribution. Circ. Res. 27 (5), 739–764.

Haidar, A., Elleri, D., Kumareswaran, K., Leelarathna, L., Allen, J.M., Caldwell, K., Murphy, H.R., Wilinska, M.E., Acerini, C.L., Evans, M.L., et al., 2013. Pharmacokinetics of insulin aspart in pump-treated subjects with type 1 diabetes: reproducibility and effect of age, weight, and duration of diabetes. Diabetes Care 36 (10), e173–e174.

Hajizadeh, I., Rashid, M., Turksoy, K., Samadi, S., Feng, J., Frantz, N., Sevil, M., Cengiz, E., Cinar, A., 2017. Plasma insulin estimation in people with type 1 diabetes mellitus. Industr. Eng. Chem. Res. 56 (35), 9846–9857.

Hajizadeh, I., Rashid, M., Cinar, A., 2019. Plasma-insulin-cognizant adaptive model predictive control for artificial pancreas systems. J. Process Control 77, 97–113.

Hovorka, R., Canonico, V., Chassin, L.J., Haueter, U., Massi-Benedetti, M., Federici, M. O., Pieber, T.R., Schaller, H.C., Schaupp, L., Vering, T., et al., 2004. Nonlinear model predictive control of glucose concentration in subjects with type 1 diabetes. Physiol. Meas. 25 (4), 905.

Kovatchev, B.P., Cobelli, C., Renard, E., Anderson, S., Breton, M., Patek, S., Clarke, W., Bruttomesso, D., Maran, A., Costa, S., Avogaro, A., Dalla Man, C., Facchinetti, A., Magni, L., De Nicolao, G., Place, J., Farret, A., 2010. Multinational study of subcutaneous model-predictive closed-loop control in type 1 diabetes mellitus: Summary of the results. J. Diab. Sci. Technol. 4 (6), 1374–1381.

Lindauer, K., Becker, R., 2019. Insulin depot absorption modeling and pharmacokinetic simulation with insulin glargine 300 u/ml. Int. J. Clin. Pharmacol. Ther. 57 (1), 1.

Poulain, C.A., Finlayson, B.A., Bassingthwaighte, J.B., 1997. Efficient numerical methods for nonlinear-facilitated transport and exchange in a blood-tissue exchange unit. Ann. Biomed. Eng. 25 (3), 547–564.

Rasmussen, C.H., Søeborg, T., Mosekilde, E., Colding-Jørgensen, M., 2011. Absorption kinetics of insulin mixtures after subcutaneous administration. In: Biosimulation in Biomedical Research, Health Care and Drug Development, Springer, pp. 329–359.

Rawlings, J.B., Mayne, D.Q., Diehl, M., 2017. Model predictive control: theory, computation, and design, Vol. 2. Nob Hill Publishing Madison.

Rodriguez-Saldana, J., 2019. The diabetes textbook: Clinical principles, patient management and public health issues. Springer.

Sangren, W., Sheppard, C., 1953. A mathematical derivation of the exchange of a labeled substance between a liquid flowing in a vessel and an external compartment. Bull. Math. Biophys. 15 (4), 387–394.

Schiavon, M., Dalla Man, C., Cobelli, C., 2017. Modeling subcutaneous absorption of fast-acting insulin in type 1 diabetes. IEEE Trans. Biomed. Eng. 65 (9), 2079–2086.

Vargas, E., Aiello, E.M., Pinsker, J.E., Teymourian, H., Tehrani, F., Church, M.M., Laffel, L.M., Doyle III, F.J., Patti, M.-E., Dassau, E., et al., 2022. Development of a novel insulin sensor for clinical decision-making. J. Diab. Sci. Technol. 19322968211071132.

Vettoretti, M., Facchinetti, A., Sparacino, G., Cobelli, C., 2015. Accuracy of devices for self-monitoring of blood glucose: A stochastic error model. 2015 37th Annual International Conference of the IEEE Engineering in Medicine and Biology Society (EMBC). IEEE, pp. 2359–2362.

Vicini, P., Bassingthwaighte, J.B., 2014. 17 - blood–tissue exchange modelling. In: Carson, E., Cobelli, C. (Eds.), Modelling Methodology for Physiology and Medicine (Second Edition). second edition Edition. Elsevier, Oxford, pp. 381–415.

Virdi, N.S., Mahoney, J.J., 2012. Importance of blood glucose meter and carbohydrate estimation accuracy. J. Diab. Sci. Technol. 6 (4), 921–926.

Visentin, R., Campos-Náñez, E., Schiavon, M., Lv, D., Vettoretti, M., Breton, M., Kovatchev, B., Dalla Man, C., Cobelli, C., 2018. The UVA/Padova type 1 diabetes simulator goes from single meal to single day. J. Diab. Sci. Technol. 12, 273–281.

Wagner, J.G., 1973. Properties of the michaelis-menten equation and its integrated form which are useful in pharmacokinetics. J. Pharmacokinet. Biopharm. 1 (2), 103–121.

Wagner, J.G., 1974. Application of the Wagner-Nelson absorption method to the two-compartment open model. J. Pharmacokinet. Biopharm. 2 (6), 469–486.

Wolkowicz, K.L., Deshpande, S., Doyle III, F.J., Dassau, E., 2020. Towards insulin monitoring: Infrequent kalman filter estimates for diabetes management. IFAC-PapersOnLine 53 (2), 15877–15883.

Wolkowicz, K.L., Aiello, E.M., Vargas, E., Teymourian, H., Tehrani, F., Wang, J., Pinsker, J.E., Doyle III, F.J., Patti, M.-E., Laffel, L.M., et al., 2021. A review of biomarkers in the context of type 1 diabetes: Biological sensing for enhanced glucose control. Bioeng. Transl. Med. 6 (2), e10201.